KCNE1 and KCNE2 Inhibit Forward Trafficking of Homomeric N-Type Voltage-Gated Potassium Channels

Vikram A. Kanda, Anthony Lewis, Xianghua Xu, and Geoffrey W. Abbott*
Department of Pharmacology, Weill Medical College of Cornell University, New York, New York

ABSTRACT Potassium currents generated by voltage-gated potassium (Kv) channels comprising α-subunits from the Kv1, 2, and 3 subfamilies facilitate high-frequency firing of mammalian neurons. Within these subfamilies, only three α-subunits (Kv1.4, Kv3.3, and Kv3.4) generate currents that decay rapidly in the open state because an N-terminal ball domain blocks the channel pore after activation—a process termed N-type inactivation. Despite its importance to shaping cellular excitability, little is known of the processes regulating surface expression of N-type α-subunits, versus their slowly inactivating (delayed rectifier) counterparts. Here we found that currents generated by homomeric Kv1.4, Kv3.3, and Kv3.4 channels are all strongly suppressed by the single transmembrane domain ancillary (β) subunits KCNE1 and KCNE2. A combination of electrophysiological, biochemical, and immunofluorescence analyses revealed this suppression is due to KCNE1 and KCNE2 retaining Kv1.4 and Kv3.4 intracellularly, early in the secretory pathway. The retention is specific, requires α-β coassembly, and does not involve the dynamin-dependent endocytosis pathway. However, the small fraction of Kv3.4 that escapes KCNE-dependent retention is regulated by dynamin-dependent endocytosis. The findings illustrate two contrasting mechanisms controlling surface expression of N-type Kv α-subunits and therefore, potentially, cellular excitability and refractory periods.

INTRODUCTION

In mammalian brain, different neuronal subtypes each display a distinct mixture of voltage-gated conductances that regulate membrane excitability (1). At the heart of this diversity lie voltage-gated potassium (Kv) channels, which open in response to cellular depolarization to repolarize the cell membrane by allowing potassium ion efflux (2). Kv channels are key determinants in the regulation of neuronal resting membrane potential, action potential duration and frequency, firing patterns, and neurotransmitter release (3,4). Augmented by alternative splicing, posttranslational modification, heteromerization of pore-forming (α) subunits, and coassembly with ancillary (β) subunits, Kv channels display a rich diversity, differing in their conductance, voltage-dependence, gating kinetics, and pharmacology (4–6). Neurons take full advantage of this diversity, using multiple Kv subunits to generate the specific repolarization profile essential to each functional niche.

Functional Kv channels can be divided into two categories defined by the degree of inactivation during depolarizing steps: delayed rectifier and fast-inactivating (7).

Delayed rectifiers activate and continue conducting K^+ ions with inappreciable to slight inactivation, even during relatively long depolarizing steps (Fig. 1 *A*) (8). This slow, C-type inactivation (also referred to as P-type or U-type depending on specific properties) is a property of almost all Kv channels, and involves structural rearrangements in either the selectivity filter or nearby residues, or a constriction of the pore (9,10). Rapidly activating delayed rectifier Kv currents produced by Kv1, Kv2, and Kv3 α-subunits generate the high K^+ permeability required for short neuronal action potentials (11–14).

Fast-inactivating Kv channels activate in response to cellular depolarization then rapidly inactivate, producing rapidly decaying currents (Fig. 1 *B*) (15,16). Three α-subunits—Kv1.4 (homologous to *Drosophila Shaker* B), and Kv3.3 and Kv3.4 (related to the *Drosophila Shaw* family)—exhibit fast-inactivating (N-type) currents because an intracellular N-terminal inactivation domain occludes the pore after channel activation (17,18). Rapid inactivation of both Kv1.4 and Kv3.4 is abolished by N-terminal deletions (19). The kinetic properties of the onset and recovery from this N-type inactivation establish refractory periods that determine excitability, firing frequency, and action potential repolarization in excitable cells (7). Kv4 subfamily subunits also inactivate rapidly, but by a mechanism considered distinct from classic N-type inactivation (20).

We previously demonstrated that KCNE1 (also named MinK) and KCNE2 (also named MinK-related peptide 1 or MiRP1), which are single-transmembrane-segment Kv channel β-subunits, form complexes with the delayed rectifier α-subunits Kv2.1, Kv3.1, and Kv3.2, resulting in functional channels bearing different activation, deactivation, and C-type inactivation properties from their α-subunit-only counterparts (21,22). We also found that KCNE3 (MiRP2) converts Kv3.4 to a subthreshold-activating channel by shifting the voltage dependence of its activation by −45 mV, and augments its current by increasing unitary conductance (23). Here we demonstrate that KCNE1 and KCNE2 suppress currents produced by the classic N-type α-subunits (Kv1.4, Kv3.3, and Kv3.4) by intracellular sequestration. In

Submitted February 7, 2011, and accepted for publication August 4, 2011.

*Correspondence: gwa2001@med.cornell.edu

Anthony Lewis's present address is School of Pharmacy and Biomedical Sciences, University of Portsmouth, Portsmouth, UK.

Editor: Eduardo Perozo.

0006-3495/11/09/1354/10 $2.00

doi: 10.1016/j.bpj.2011.08.015

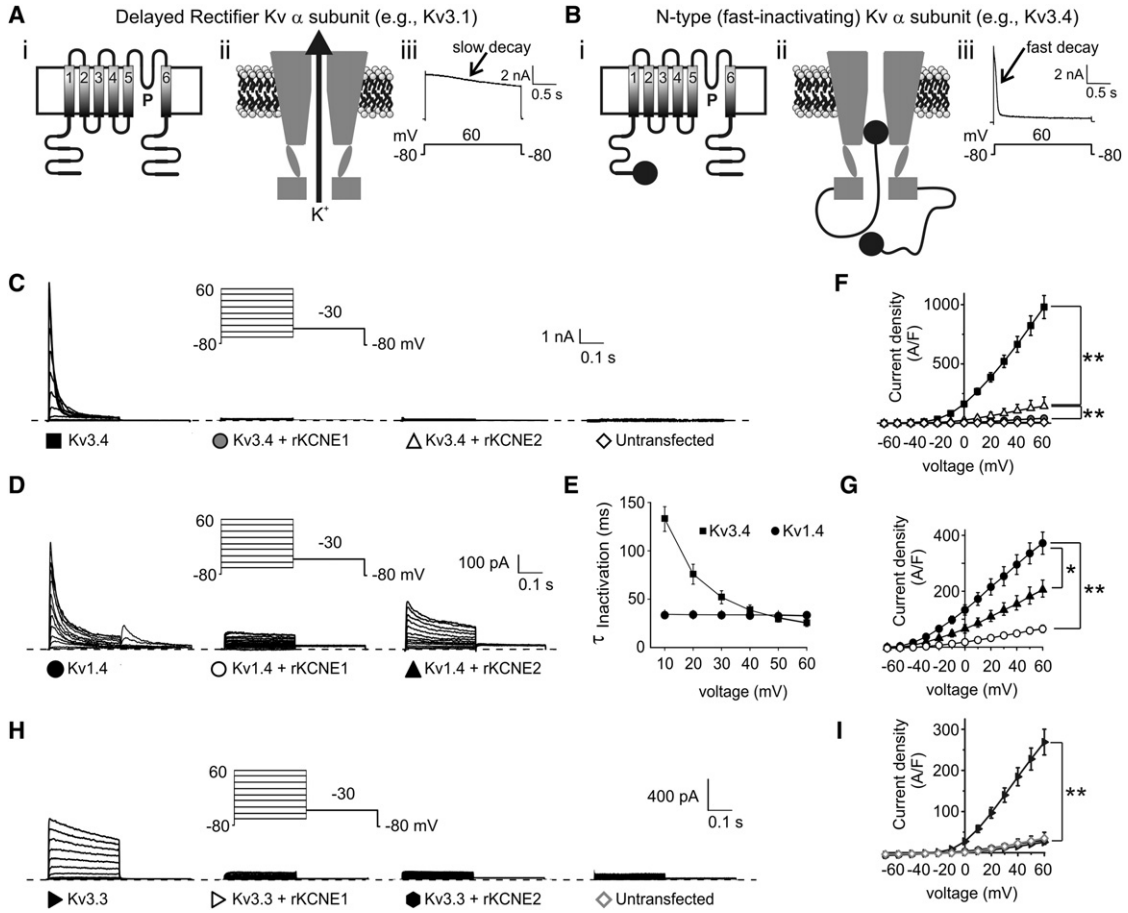

FIGURE 1 KCNE1 and KCNE2 suppress N-type K^+ currents. (*A*) Schematic of delayed rectifier Kv channel α-subunits. (*i*) Membrane topology of a delayed rectifier Kv α-subunit. (*ii*) Cross section through delayed rectifier Kv channel α-subunits highlighting the ion conduction pathway. (*iii*) Exemplar current trace at + 60 mV of Kv3.1 using the inset protocol. (*B*) Schematic of N-type Kv channel α-subunits. (*i*) Membrane topology of an N-type Kv α-subunit, with the ball domain highlighted. (*ii*) Cross section through N-type Kv channel α-subunits highlighting the ion conduction pathway being blocked by the N-terminal ball domain. (*iii*) Exemplar current trace at + 60 mV of Kv3.4 using the inset protocol. (*C*) Exemplar traces showing currents recorded in CHO cells from untransfected cells and cells transfected with Kv3.4 alone or with rat KCNE1 or KCNE2 as indicated. (*Inset*) Voltage protocol. (*D*) Exemplar traces showing currents recorded in CHO cells transfected with Kv1.4 alone or cotransfected with rat KCNE1 or KCNE2 as indicated. (*Inset*) Voltage protocol. (*E*) Mean inactivation rates for homomeric Kv3.4 and Kv1.4 at voltages between +10 mV and +60 mV, fitted with a single exponential function, expressed as $\tau_{inactivation}$. (*F*) Mean peak current density from CHO cells transfected with Kv3.4 alone ($n = 30$), or with KCNE1 ($n = 15$), KCNE2 ($n = 15$), or untransfected cells ($n = 10$); symbols as in panel *C*. $^{**}p < 0.001$. (*G*) Mean peak current density from CHO cells transfected with Kv1.4 alone ($n = 20$) or with KCNE1 ($n = 18$) or KCNE2 ($n = 12$); symbols as in panel *E*. $^{*}p < 0.05$; $^{**}p < 0.001$. (*H*) Exemplar traces showing currents recorded in CHO cells from untransfected cells and cells transfected with Kv3.3 alone or with rat KCNE1 or KCNE2 as indicated. (*Inset*) Voltage protocol. (*I*) Mean peak current density from CHO cells transfected with Kv3.3 alone ($n = 8$), or with KCNE1 ($n = 8$), KCNE2 ($n = 8$), or untransfected cells ($n = 10$); symbols as in panel *H*. $^{**}p < 0.001$.

a companion article in this issue, we demonstrate how this mechanism can be utilized by the cell to regulate the α-subunit composition of surface-expressed channels.

MATERIALS AND METHODS

Cell culture and transfection

Chinese hamster ovary (CHO) cells were cultured in F12K medium (containing L-glutamine and sodium bicarbonate; American Type Culture Collection, Manassas, VA) supplemented with 10% fetal bovine serum (Invitrogen, Carlsbad, CA) and 1% penicillin and streptomycin, incubated at 37°C and gassed with 5% CO_2. CHO cells were cultured in 10-cm tissue culture dishes. When near confluent, the monolayer was washed once with Ca^{2+}- and Mg^{2+}-free Dulbecco's phosphate-buffered saline (Invitrogen) and incubated with 0.05% Trypsin-EDTA (MP Biomedical, Solon, OH) for 5 min. The cells were then centrifuged at 1000 RPM for 5 min and resuspended in supplemented F12K medium. For transfections, 5×10^5 cells were plated in 60-mm tissue culture dishes one day before transfection.

To study Kv channels in the presence and absence of KCNEs, CHO cells were transiently transfected using SuperFect transfection reagent (Qiagen, Hilden, Germany) following the manufacturer's protocol. Cells were transfected with cDNA as follows (per 60 mm dish): 0.1 μg of rat α-subunit cDNA alone or in combination with 0.5 μg of β-subunit cDNA (rat unless otherwise noted), and an empty vector (pBluescript) to enhance transfection efficiency. Cells were also cotransfected with a plasmid cDNA encoding enhanced green fluorescent protein (pBOB-EGFP) to visualize transfected cells for whole cell voltage-clamp experiments. Experiments were carried out 24 h posttransfection. For protein biochemistry, hemagglutinin (HA)-tagged constructs of KCNE1 and KCNE2 were used to facilitate detection (as used previously (21)).

Electrophysiology

Electrophysiological recordings from transiently-transfected CHO cells were performed by voltage-clamp using the whole cell configuration of the patch-clamp technique as previously described in Lewis et al. (21). Briefly, whole-cell currents were recorded using a Multiclamp 700A amplifier (Axon Instruments, Foster City, CA) and data acquisition and analysis were performed using the pCLAMP 9.0 software suite (Axon Instruments). Cells were perfused with an extracellular bath solution containing 135 mM NaCl, 5 mM KCl, 1.2 mM $MgCl_2$, 5 mM HEPES, 2.5 mM $CaCl_2$, 10 mM D-glucose (pH 7.4). Patch electrodes were pulled from standard-walled, borosilicate glass capillaries with filament (Sutter Instruments, Novato, CA) using a P-97 horizontal puller (Sutter Instruments) and had resistances of 3–5 MΩ when filled with intracellular solution containing 10 mM NaCl, 117 mM KCl, 2 mM $MgCl_2$, 11 mM HEPES, 11 mM EGTA, 1 mM $CaCl_2$ (pH 7.2). Data were filtered at 1 kHz and digitized at 5 kHz using a Digidata 1322A analog-to-digital converter (Axon Instruments).

All recordings were performed using the following voltage protocol: From a holding voltage of −80 mV, cells were pulsed at voltages between −60 mV and +60 mV in 10 mV increments for 300 ms, followed by 300 ms tail pulse at −30 mV, unless otherwise noted. Leak and liquid potentials were not compensated for. For Kv3.4 and Kv1.4, the time constant of inactivation ($\tau_{inactivation}$) was calculated from the peak of the evoked current to a point corresponding to the steady state of inactivation, and fit by a single exponential equation ($I(t) = A_1 e^{(-t/\tau 1)}$). Data were analyzed using Clampfit 9.0 software (Axon Instruments) and graphs were generated using Origin 6.0 (Microcal, Northampton, MA). Data are expressed as means ± SE of observations from n cells. Statistical significance was assessed by one-way analysis of variance with $p < 0.05$ being indicative of significance.

Protein biochemistry

Coimmunoprecipitation studies were performed using a protocol adapted from Lewis et al. (21). Briefly, CHO cells were lysed 24 h posttransfection in lysis buffer: 150 mM NaCl, 50 mM Tris-HCl (pH 7.4), 20 mM NaF, 10 mM Na_3VO_4, 1% Nonidet P-40 (Pierce, Rockford, IL), 1% CHAPS (Sigma, St. Louis, MO), 1% Triton X-100 (Fisher Scientific, Pittsburgh, PA), 0.5% sodium dodecyl sulfate (Sigma), and one mini-complete protein inhibitor cocktail tablet per 10 ml (Roche Applied Science, Indianapolis, IN). The lysis was carried out for 2 h at 4°C. The supernatants were then precleared with protein A/G PLUS-agarose immunoprecipitation reagent (Santa Cruz Biotechnology, Santa Cruz, CA) for 20 min at 4°C; these beads were collected by centrifugation at 1000 × g for 5 min and discarded. Precleared supernatants were incubated with antibodies for immunoprecipitation: rabbit polyclonal anti-Kv3.4 (Sigma) or mouse monoclonal anti-HA-7 (Sigma). After 5–12 h at 4°C, protein A/G PLUS-agarose beads were added and the mixture incubated for a further 2 h at 4°C.

The beads were washed for 4 × 15 min, then immunopurified complexes were eluted by incubating the beads for 20 min at 37°C in SDS-PAGE loading buffer (Bio-Rad Laboratories, Hercules, CA), with vigorous vortexing directly before and after the incubation. After centrifugation, the bead eluates were separated by SDS-PAGE on 4–20% gels. After transfer onto PVDF membranes, blots were probed with either monoclonal mouse anti-HA antibodies or polyclonal rabbit anti-Kv3.4 antibodies (Sigma) overnight at 4°C. For secondary detection, horseradish peroxidase-conjugated species-appropriate anti-IgG antibodies (Bio-Rad) were utilized. Lastly, signals were detected using ECL Western Blotting Substrate (Pierce).

For surface biotinylation experiments, CHO cells were transfected 24 h before biotinylation. The cells were washed three times with ice-cold phosphate-buffered saline (PBS) (pH 8.0), then incubated in PBS containing Sulfo-NHS-LC-biotin (Pierce) (0.5 mg/ml in PBS) for 30 min on ice. The biotin was quenched with three washes of ice-cold 100 mM glycine buffer. After washing, the cells were lysed in lysis buffer as described above. Biotinylated proteins were then pulled-down by incubation with high-capacity Streptavidin beads (Pierce) overnight at 4°C. The beads were washed 4 × 10 min and eluted with SDS-PAGE loading buffer and separated by SDS-PAGE. Western blots were performed as described above.

For deglycosylation experiments, PNGase F (New England Biolabs, Ipswich, MA) and Endo H_f (New England Biolabs) were used to analyze N-linked glycosylation using the manufacturer's protocol. Briefly, cells were lysed as described above. The lysates were mixed with 10× glycoprotein denaturing buffer and heated to 100°C for 10 min. For Endo H_f experiments, 10× G5 reaction buffer with Endo H_f was then added. For PNGase F experiments, 10× G7 reaction buffer and 10% NP-40 were added along with PNGase F. The reactions were incubated for 60 min at 37°C and then run on SDS-PAGE gels as described above.

Immunofluorescence and colocalization analysis

For immunofluorescence experiments, CHO cells were transfected as described above, but with an additional 1 μg cDNA of a fluorescent marker for cell organelles (Clontech Laboratories, Mountain View, CA) as follows: endoplasmic reticulum (ER), pDsRed2-ER; Golgi, pDsRed-Monomer-Golgi. After transfection, the cells were lysed and moved from 60 mm dishes to a Culturewell chambered cover glass (Invitrogen). After 24 h, the cells were washed once in PBS and fixed in ice-cold 4% paraformaldehyde in PBS for 30 min at room temperature. The cells were then washed twice with ice-cold PBS for 1 min each wash. The cells were subsequently permeabilized using 0.25% Triton-X-100 in PBS for 10 min at room temperature and washed 3 × 5 min in PBS.

After blocking the cells for 30 min in 1% bovine serum albumin (BSA)/phosphate-buffered saline (PBS), the cells were incubated with primary antibodies for 1 h at room temperature. Rabbit polyclonal anti-Kv3.4 or anti-Kv1.4 (1:300; Sigma) or mouse monoclonal anti-HA 7 (1:1000; Sigma) were utilized. The cells were again rinsed and incubated with secondary antibodies (1:1000; Alexa Fluor 488 donkey anti-rabbit IgG (H+L) or Alexa Fluor 350 donkey anti-mouse IgG (H+L)) in 1% BSA/PBS in the dark for 1 h at room temperature. The cells were washed again 3 × 5 min in PBS, then mounted on slides in Prolong anti-fade mounting medium (Invitrogen). The slides were allowed to set overnight before viewing on a BX51 upright epifluorescence microscope (Olympus, Tokyo, Japan) using cellSens Standard digital imaging software (Olympus). Images were acquired using a 100× oil-immersion lens.

Colocalization of proteins and intracellular markers from images taken by epifluorescence microscopy was quantified using Pearson's correlation coefficient (PCC), as previously used by others to quantify protein colocalization from epifluorescence images (24–28). Specifically, PCC values were determined by intensity correlation analysis (ICA) (29) with ImageJ software (National Institutes of Health (NIH), Bethesda, MD), using the MBF ImageJ for Microscopy collection of plug-ins (McMaster Biophotonics Facility, Hamilton, Ontario, Canada). PCC (R_r), a well-characterized and well-established method to measure correlation in imaging, determines the degree to which two color channels overlap (30). PCC is determined by the following equation:

$$R_r = \frac{\sum (R_i - R_{av}) * (G_i - G_{av})}{\sqrt{\sum (R_i - R_{av})^2 * \sum (G_i - G_{av})^2}}.$$

Here, R_i is the fluorescent intensity of one color channel (e.g., *red*) and R_{av} is the arithmetic mean. G, in this case, indicates the second (e.g., *green*) color channel in the same pixels. The denominator indicates perfect correlation. The numerator indicates the sum total of each fluorophore in the same pixels. For imaging, PCCs typically range from 1, representing perfect correlation, to −1, generally representing perfect exclusion if in the linear range. Though low and negative R_r values in imaging can be difficult to interpret, a positive value nearer to 1 indicates reliable colocalization.

The two images to be quantified were first opened using the software ImageJ (NIH). Extracellular fluorescent background was then subtracted from the images, by selecting a background region-of-interest (ROI) and

then subtracting it from each stack. The images were subsequently converted to an eight-bit grayscale. An ROI was then selected that only encompassed the cell to be analyzed, minimizing background. ICA was performed on the selected ROI in both images. ICA generates a frequency scatter plot and generates an R_r value. Pixels with a value of zero in both color channels are ignored as background. The R_r values from at least five cells were averaged from at least five cells to accurately represent each correlation. A positive control for the colocalization correlation was performed by labeling each protein with two different primary antibodies and two different secondary antibodies, examining the colocalization of the two probes.

For controls, Kv3.4 was also labeled using a mouse monoclonal Kv3.4 antibody (clone N72/16, 1:300 NeuroMab; University of California at Davis/NIHNeuroMab Facility, Davis, CA). KCNE1 was also labeled with a rabbit polyclonal KCNE1 antibody (1:100; Alomone Labs, Jerusalem, Israel), and Kv1.4 was also labeled with a mouse monoclonal Kv1.4 antibody (1:250, clone K13/31, 1:300, NeuroMab). A negative control was also performed for the colocalization correlation, under the same conditions as for the positive control but with one image rotated 90° in relation to the other. Lastly, where indicated, scatter plots of the fluorescence intensity of each probe in representative images were determined, again through ICA (29) with Image J software (NIH), using the MBF ImageJ for Microscopy collection of plug-ins (McMaster Biophotonics Facility).

RESULTS

KCNE1 and KCNE2 suppress N-type currents

CHO cells transfected with Kv3.4, Kv1.4, or Kv3.3 cDNA alone exhibited rapidly activating and inactivating currents, measured using whole-cell voltage clamp (Fig. 1, *C*, *D*, and *H*). Consistent with previous reports (3,31), homomeric Kv3.4 inactivation rate was voltage-dependent, with the inactivation time constant ($\tau_{inactivation}$) decreasing from 133 ± 13 ms at +10 mV to 26 ± 4 ms at +60 mV; in contrast, homomeric Kv1.4 inactivation rate was voltage-independent ($\tau_{inactivation}$ was 33 ± 2 ms regardless of voltage; see Fig. 1 *E*).

We previously demonstrated that KCNE3 increases the unitary conductance and voltage-dependent open probability of Kv3.4 in CHO cells (23). In contrast, here, cotransfection of KCNE1 or KCNE2 (cloned from rat) suppressed Kv3.4 current >95% ($p < 0.001$; Fig. 1, *C* and *F*). Kv1.4 current density was also suppressed: 80% by KCNE1 ($p < 0.001$) and almost 50% by KCNE2 ($p < 0.05$; Fig. 1, *D* and *G*). Cotransfection of KCNE1 or KCNE2 also suppressed Kv3.3 current >90% ($p < 0.001$; Fig. 1, *H* and *I*). Cells transfected with Kv3.3 alone displayed slower inactivation than Kv3.4 and Kv1.4 in our system, consistent with previous reports that Kv3.3 inactivation rate is highly dependent on regulation, expression system, and possibly initiation site (32,33).

KCNE1 and KCNE2 inhibit Kv3.4 and Kv1.4 surface expression

We next examined possible mechanisms of inhibition, focusing first on Kv3.4 because of the comprehensive nature of its suppression by KCNE1 and KCNE2. Western blots of lysates from CHO cells expressing Kv3.4 alone showed two bands, indicating two different molecular mass species, expressed at 75 and 100 kDa (*arrows*), with the heavier band enriched in the surface fraction, as determined by surface biotinylation (Fig. 2 *A*). Significantly, coexpression of KCNE1 decreased the relative intensity of the upper band in whole cell lysates, and greatly reduced Kv3.4 surface expression (Fig. 2 *A*).

Kv3.4 reportedly has two conserved *N*-glycosylation sites (34). To investigate the source of the size shift in Kv3.4 concurrent with KCNE1 coexpression, we treated lysates with two different deglycosylation agents: Endoglycosidase H (Endo H) or the peptide *N*-glycosidase F (PNGase F). Endo H cleaves only N-linked high mannose-type sugars found on immature proteins in the ER, whereas PNGase F cleaves all N-linked sugars, including those cleaved by Endo H and those found on more mature proteins that have progressed past the ER and into the Golgi (35). In lysates from cells overexpressing solely Kv3.4, Endo H treatment did not alter migration of the upper (100 kDa) band, but increased the migration distance of the 75 kDa band to 68 kDa (Fig. 2 *B*).

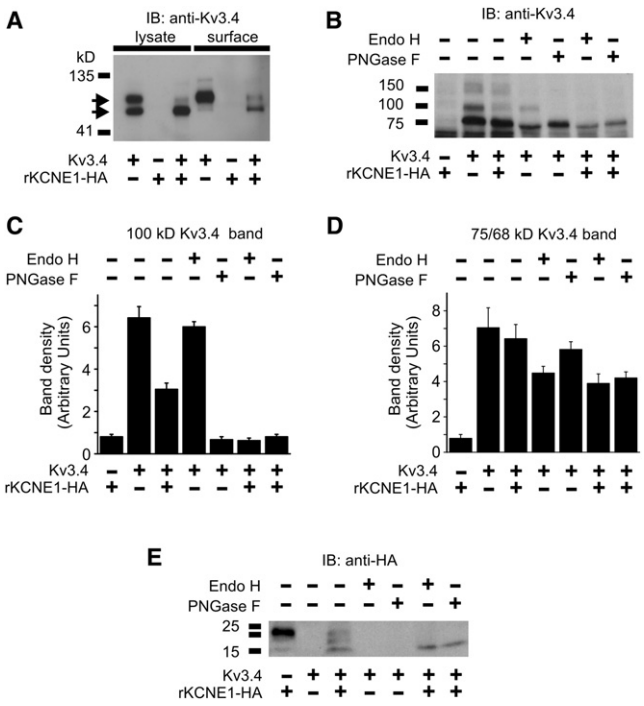

FIGURE 2 Rat KCNE1 suppresses Kv3.4 current by inhibiting surface expression. (*A*) Western blot, using anti-Kv3.4 antibody, of cell lysates and avidin-biotin-purified surface fractions from CHO cells transfected with Kv3.4 and/or rKCNE1-HA (indicated by + and – symbols). (*Arrows*) Two observed molecular mass species of Kv3.4. (*B–D*) Deglycosylation analysis of Kv3.4. CHO cells were transfected with cDNAs as indicated by the + and – symbols below the fluorograph. The + and – symbols above the fluorography indicate use of deglycosylation agents. (*B*) Representative Western blot. (*C*) 100 kDa Kv3.4 band density for $n = 3$ blots as in panel *B*. (*D*) 75/68 kDa Kv3.4 band density for $n = 3$ blots as in panel *B*. (*E*) Deglycosylation analysis of rat KCNE1. Cells were transfected with cDNAs as indicated by the + and – symbols below the fluorograph. The + and – symbols above the fluorography indicate use of deglycosylation agents.

In contrast, PNGase F treatment completely collapsed the 100 kDa band to 75 kDa, without generating a band at 68 kDa (Fig. 2, *B* and *C*)—confirming results previously reported by others (34). Quantitative comparison of the 100 kDa band in Endo-H treated versus nontreated samples expressing similar subunits showed no significant difference in band density (Fig. 2 *C*). In nonglycosidase-treated samples, coexpression of KCNE1 reduced the density of the 100 kDa Kv3.4 band twofold (Fig. 2 *C*). Glycosidase treatment had a general (nonspecific) effect of reducing density of the faster-migrating Kv3.4 band, probably arising from degradation due to, e.g., high temperature and/or prolonged incubations, but band densities after treatment were still >4-fold greater than for non-Kv3.4-transfected, nontreated controls (Fig. 2 *D*).

The shift in band pattern arising from PNGase F treatment, but not that arising from Endo H treatment, mimicked the effects of KCNE1 cotransfection. This suggested that KCNE1 reduced expression of mature Kv3.4 (100 kDa band), but did not inhibit intra-ER processing of Kv3.4 (which would have mimicked Endo-H treatment and shifted the 75 kDa band to 68 kDa). Cotransfection with Kv3.4 also altered the SDS-PAGE migration pattern of KCNE1. When expressed alone, KCNE1 was predominantly in the high molecular mass (biglycosylated) form, whereas Kv3.4 coexpression resulted in equal distribution between non, mono, and biglycosylated forms (Fig. 2 *E*). The data suggested KCNE1 inhibited Kv3.4 surface expression, and that processing of either subunit was altered by coexpression of the other.

Considering once more Fig. 2 *A*, when KCNE1 was coexpressed, the 75 kDa Kv3.4 band was slightly more prominent than the 100 kDa Kv3.4 band. Yet compared to the corresponding lysate band pattern, the lower band was greatly reduced in intensity whereas the upper surface band was of similar intensity to the upper lysate band. Existence of the 75-kDa, presumably immature, form of Kv3.4 apparently at the cell surface can be explained by at least two possibilities: first, it is known that surface biotinylation is often a less-than-perfect assay because some biotin can be internalized by endocytosis and can thus label proteins intracellularly; and second, coexpression of KCNE1 may alter Kv3.4 trafficking such that some of the latter reaches the surface despite not being glycosylated fully or correctly.

Immunofluorescence studies (Fig. 3) supported the conclusion that KCNE1 inhibits Kv3.4 forward trafficking. When expressed alone, Kv3.4 localized strongly at the plasma membrane and accumulated less in the ER (Pearson's correlation coefficient for Kv3.4 and the ER marker $= 0.58 \pm 0.03$, $n = 5$; Fig. 3, *A* and *H*). A positive control for the correlation coefficient was performed by labeling Kv3.4 with two different primary antibodies (Pearson's correlation coefficient for Kv3.4 $= 0.92 \pm 0.02$, $n = 5$; Fig. 3, *B* and *C*). A negative control for the correlation coefficient was also performed by rotating one of these images 90° in relation to the other; here, the Pearson's correlation coefficient approached zero (0.012 ± 0.0008, $n = 5$; Fig. 3 *C*). These control values validated the use of Pearson's to quantify colocalization of fluorescently-labeled proteins imaged using epifluorescence microscopy.

In contrast, when expressed alone, rat KCNE1 localized almost exclusively intracellularly in the ER (Pearson's correlation coefficient for KCNE1 and the ER marker $= 0.90 \pm 0.006$, $n = 5$; Fig. 3, *D* and *H*). Positive and negative controls for the correlation coefficient were also performed by labeling KCNE1 with two different antibodies (Fig. 3, *E* and *F*), with similar results as obtained for Kv3.4 (Fig. 3, *B* and *C*). Coexpression of Kv3.4 and rat KCNE1 resulted in strong suppression of Kv3.4 surface expression, which was instead located primarily intracellularly, colocalizing strongly with the ER and with KCNE1; this was evident by the strong white signal on the triple colocalized image, compared to a much fainter green signal, indicating a minority of Kv3.4, at or near the cell surface (Fig. 3 *G*). This strong colocalization of Kv3.4 with the ER and KCNE1 was also evident from quantification using correlation analysis, which gave a Pearson's correlation coefficient of >0.9 in each case (Fig. 3 *H*).

Similar results were obtained when quantifying the presence of these subunits in the Golgi, although to a lesser degree (see Fig. S1 in the Supporting Material). We speculate that this Golgi colocalization results from saturation of available sites in the ER. Likewise, rat KCNE2 intracellularly sequestered Kv3.4, the two localizing strongly together in the ER and to a lesser extent in the Golgi (see Fig. S2). Interestingly, unlike rat KCNE1, a fraction of rat KCNE2, when coexpressed with Kv3.4, reached the cell surface alone (see Fig. S2). This is consistent with previous reports that KCNE2 can traffic to the plasma membrane alone, unlike KCNE1 (36).

KCNE1-mediated suppression of Kv1.4 appeared to occur through a similar mechanism. When expressed alone, Kv1.4 localized both to the plasma membrane and intracellularly, albeit with a relatively low Kv1.4-ER Pearson's correlation coefficient of <0.6 (see Fig. S3, *A* and *F*). Positive and negative colocalization controls for the Pearson's correlation coefficient were performed by labeling Kv1.4 with two different antibodies, giving a value approaching 1, versus a value close to 0 when one of the images was rotated 90° before calculation of the coefficient (see Fig. S3, *B* and *C*).

Coexpression of rat KCNE1 with Kv1.4 greatly increased colocalization of Kv1.4 with the ER, as indicated by a white signal in triple-merged immunofluorographs and a Pearson's correlation coefficient of 0.96 ± 0.02 ($p < 0.05$ compared to value for Kv1.4 in the absence of KCNE1, $n = 5$; see Fig. S3, *D* and *F*). Under these conditions, we still detected some Kv1.4 at the membrane alone, consistent with the electrophysiological data (Fig. 1 *D*; and see Fig. S3 *D*).

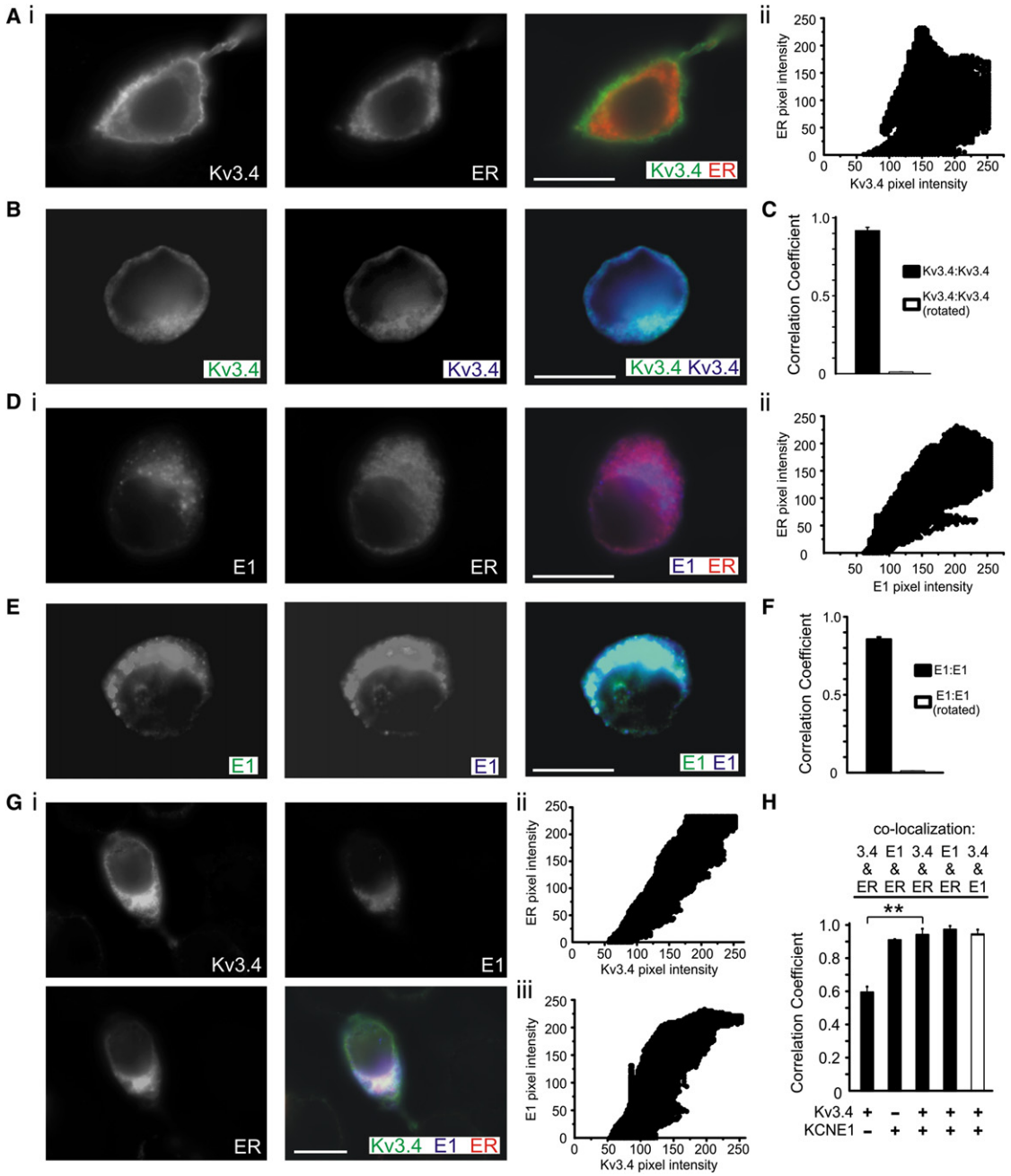

FIGURE 3 Rat KCNE1 retains Kv3.4 intracellularly. Immunofluorescence analysis of CHO cells transfected with Kv3.4 (*green*), fluorescent ER marker (*red*), and rat KCNE1-HA (*blue*) as indicated. Scale bars: 5 μm. Representative images, taken from at least five images per group, are shown. Single-wavelength images are shown in monochrome for clarity; double- and triple-wavelength, merged images are shown in color. (*A*) Kv3.4 transfected without KCNE1 or KCNE2. (*i*) Representative images. (*ii*) Fluorescence intensities for the representative images are displayed as scatter plots. (*B*) Representative images of Kv3.4 positive control (Kv3.4 transfected without KCNE1 or KCNE2, labeled with two different antibodies to Kv3.4). (*C*) Quantification of colocalization from images as in panel *B* using Pearson's correlation coefficient, $n = 5$ cells per group, as indicated, For a negative control, one image per group as in panel *B* was rotated 90° and the correlation coefficient recalculated. (*D*) KCNE1 transfected without Kv3.4. (*i*) Representative images. (*ii*) Fluorescence intensities for the representative images are displayed as scatter plots. (*E*) Representative images of KCNE1 colocalization positive control (KCNE1 transfected without Kv3.4, labeled with one antibody raised against the HA tag on KCNE1, and one raised against a native epitope on KCNE1). (*F*) Quantification of colocalization from images as in panel *E* using Pearson's correlation coefficient, $n = 5$ cells per group, as indicated. For a negative control, one image per group as in panel *E* was rotated 90° and the correlation coefficient recalculated. (*G*) Kv3.4 and KCNE1 cotransfected. (*i*) Representative images. In the color, merged image, triple colocalization is observed as a white signal. Fluorescence intensities for the representative images are displayed as scatter plots: (*ii*) ER versus Kv3.4. (*iii*) KCNE1 versus Kv3.4. (*H*) Quantification of colocalization from images as in panels *A*, *B*, *D*, *E*, and *G* using Pearson's correlation coefficient, $n = 5$ cells per group, ** $p < 0.001$.

Coexpression of rat KCNE2 and Kv1.4 also increased colocalization of Kv1.4 with the ER, compared to Kv1.4 expressed alone ($p < 0.05$; Pearson's correlation coefficient for Kv1.4 and ER when comparing cells with-versus-without KCNE2 coexpression; $n = 5$; Fig. 3, *A*, *E*, and *F*). This ER localization was not as strong as that induced by KCNE1 coexpression. However, in these cells, some surface-expressed Kv1.4 and KCNE2 was also apparent, some colocalized with one another and some not (see Fig. 3 *E*). This tallied with the less-efficient current inhibition of Kv1.4 by rat KCNE2 compared to rat KCNE1, suggesting that the mechanism and/or efficiency of Kv1.4 inhibition by KCNE2 is somewhat different than for KCNE1, and again supported the notion that KCNE2 can reach the cell surface alone, unlike KCNE1. Kv1.4 colocalized reasonably strongly with both rat KCNE1 and KCNE2 (see Fig. S3 *G*), and coimmunoprecipitation studies confirmed that Kv1.4 formed complexes both with rat KCNE1 and rat KCNE2 (Fig. 4 *A*).

KCNE2-mediated suppression of Kv3.4 requires their coassembly

We previously showed that in CHO cells, rat KCNE2 altered the activation, deactivation, and inactivation of rat Kv3.1 and Kv3.2, whereas the human variant of KCNE2 had no effect despite efficient human KCNE2 expression, due to an inability to interact with these α-subunits in the CHO cell expression system (21). Here, we exploited this species difference to determine whether Kv3.4 suppression by KCNEs required intersubunit interaction, versus it being an artifact of heterologous overexpression. Coimmunoprecipitation studies showed that Kv3.4 formed complexes with rat KCNE1 and rat KCNE2, but not with human KCNE2 (Fig. 4 *C*), despite detectable human KCNE2 expression (Fig. 4 *B*).

Accordingly, and unlike with rat KCNE1 and KCNE2, human KCNE2 had no effect on Kv3.4 current (Fig. 4, *D* and *E*), and failed to inhibit Kv3.4 surface expression (Fig. 4 *F*). Hence, the Pearson's correlation coefficient for colocalization of Kv3.4 with the ER remained at ~0.6 whether in the presence (Fig. 4 *G*) or absence (Fig. 3 *H*) of human KCNE2. Thus, merely the presence of a KCNE subunit was not sufficient for inhibition of Kv3.4 forward trafficking; rather, KCNE-Kv3.4 complex formation was required for suppression. Further studies are required to determine which of the 22/123 residues that differ between rat and human KCNE2, situated mostly in the predicted KCNE2 intracellular and extracellular domains, are

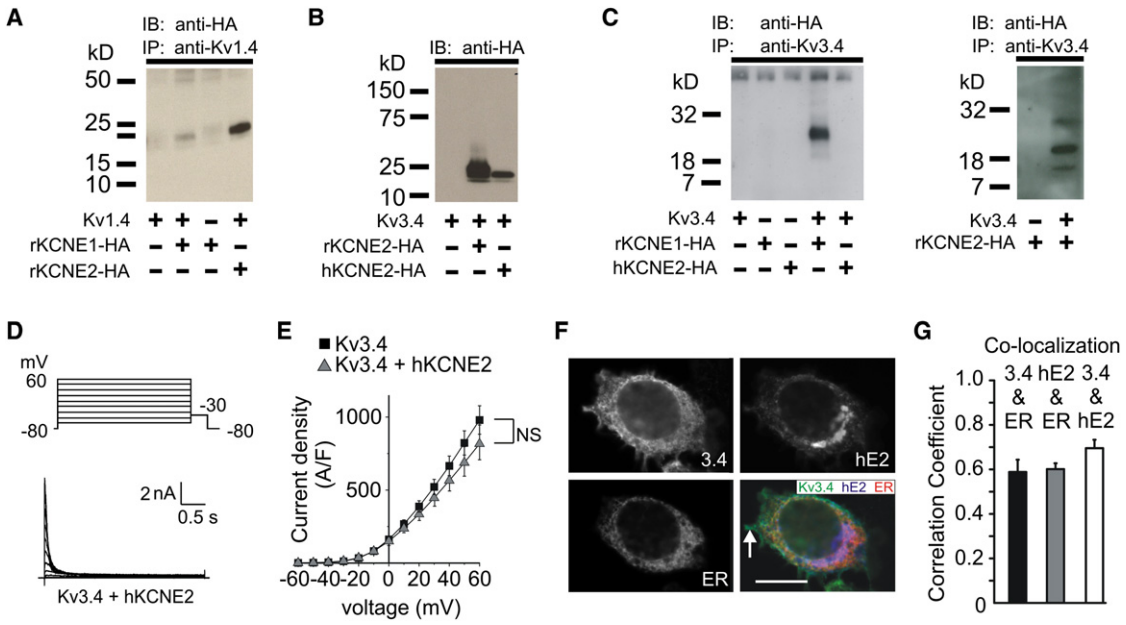

FIGURE 4 Human KCNE2 does not coassemble with Kv3.4 or alter its currents or surface expression in CHO cells. (*A*) Western blot of CHO cell lysates after immunoprecipitation (*IP*) with anti-Kv1.4 antibody, showing Kv1.4 forms complexes with rat KCNE1 and rat KCNE2 (each tagged with HA epitope and immunoblotted (*IB*) with anti-HA antibody). Cells were transfected with subunit cDNAs as indicated by the + and – symbols. (*B*) Western blot of CHO cell lysates showing expression of rat KCNE2 and human KCNE2 when coexpressed with Kv3.4. Cells were transfected as indicated by the + and – symbols. (*C*) Western blots of CHO cell lysates after immunoprecipitation (*IP*) with anti-Kv3.4 antibody, and immunoblotted (*IB*) with anti-HA antibody, showing Kv3.4 forms complexes with rat KCNE1, rat KCNE2, but not human KCNE2. Cells were transfected as indicated by the + and – symbols. (*D*) Exemplar trace showing current recorded in CHO cells cotransfected with Kv3.4 and human KCNE2, using the inset voltage protocol. (*E*) Mean peak current density from CHO cells transfected with Kv3.4 alone (*solid squares, n* = 8) or with human KCNE2 (*gray triangles, n* = 10). (*F*) Exemplar IF colabeling of Kv3.4 (*green*) and human KCNE2-HA (*blue*); fluorescent ER marker (*red*). Scale bar = 5 μm. Representative images, taken from at least five images per group, are shown. Single-wavelength images are shown in monochrome for clarity; the triple-wavelength, merged image is shown in color. (*Arrow*) Kv3.4 at the cell surface. (*G*) Quantification of colocalization from images as in panel *F* using the Pearson's correlation coefficient, $n = 5$ cells per group.

responsible for the inability of the former to coassemble with Kv3 subunits, and how specific this is to the α-subunit species and expression system.

KCNE1 does not suppress Kv3.4 current primarily by promoting endocytosis

Previously, we found that KCNE1 directed the dynamin-dependent endocytosis (DDE) of KCNQ1 (Kv7.1), a delayed-rectified Kv α-subunit (37). To determine whether KCNE1 and KCNE2 were decreasing Kv3.4 surface expression by increasing DDE rather than, or in addition to, inhibiting forward trafficking as data in Figs. 2 and 3 suggest, we performed a series of experiments using dominant-negative K44A dynamin 2, which inhibits clathrin-mediated endocytosis and other forms of DDE (38). Coexpression of K44A dynamin 2 increased the current threefold compared to that with Kv3.4 and rat KCNE1 alone ($p < 0.001$; Fig. 5,

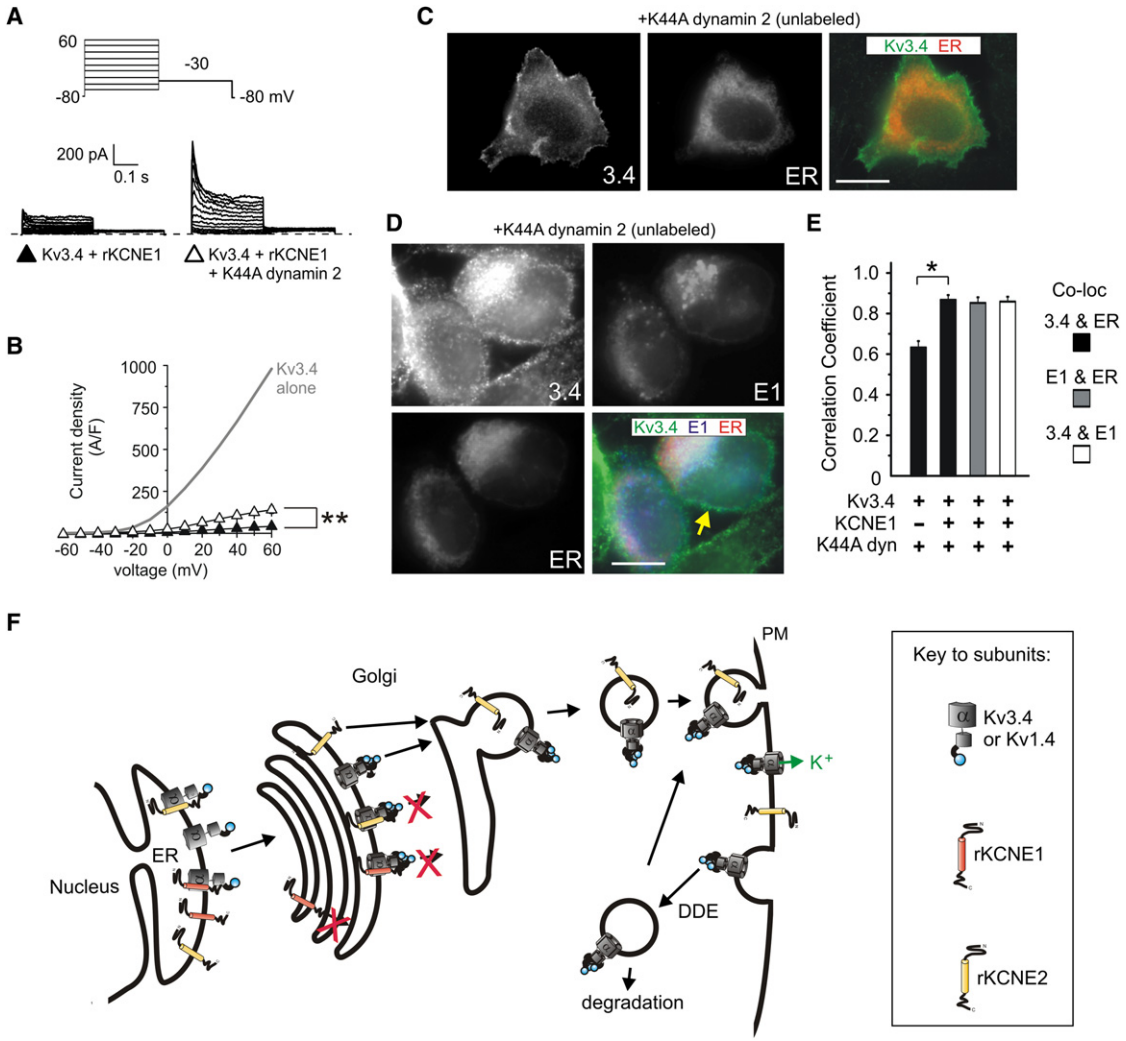

FIGURE 5 KCNE1 does not inhibit Kv3.4 surface expression via dynamin-dependent endocytosis. (*A*) Exemplar traces showing currents recorded in CHO cells cotransfected with Kv3.4 and rat KCNE1, with or without K44A dynamin 2 as indicated. (*Inset*) Voltage protocol. (*B*) Mean peak current density from CHO cells cotransfected with Kv3.4 and rat KCNE1 ($n = 10$) or cotransfected with Kv3.4, rat KCNE1 and K44A dynamin 2 ($n = 10$); symbols as in panel *A*. ** $p < 0.001$. Plot for Kv3.4 alone (from Fig. 1) shown for comparison (*gray line*). (*C*) Exemplar IF colabeling of cells transfected with Kv3.4 (*green*), K44A dynamin 2 (not stained), and a fluorescent ER marker (*red*). Scale bar: 3 μm. Representative images, taken from at least five images per group, are shown. Single-wavelength images are shown in monochrome for clarity; the double-wavelength, merged image is shown in color. (*D*) Exemplar IF colabeling of cells transfected with Kv3.4 (*green*), K44A dynamin 2 (not stained), rat KCNE1-HA (*blue*), and a fluorescent ER marker (*red*). Scale bar: 3 μm. Representative images, taken from at least five images per group, are shown. Single-wavelength images are shown in monochrome for clarity; the triple-wavelength, merged image is shown in color. The merged image shows strong triple colocalization (*white signal*) of Kv3.4, KCNE1 and in the ER, and some lower-intensity Kv3.4 staining (*green signal*) at the plasma membrane (*yellow arrow*). (*E*) Quantification of colocalization from images as in panels *C* and *D* using Pearson's correlation coefficient, $n = 5$ cells per group. * $p < 0.05$. (*F*) Model of N-type α-subunit suppression by rat KCNE1 and rat KCNE2. Rat KCNE1 and rat KCNE2 retain N-type α-subunits in the Golgi and/or ER, preventing their forward-trafficking and surface expression. The few Kv3.4 subunits that escape retention reach the plasma membrane (*PM*) and are then available for internalization by dynamin-dependent endocytosis (*DDE*). Whereas lone KCNE1 is retained in the ER and/or Golgi, lone KCNE2 can travel to the cell surface.

A and *B*). This current displayed N-type inactivation, but was still 85% smaller than that produced by Kv3.4 alone ($p < 0.001$; Figs. 1 *C* and 5 *B*).

Immunofluorescence studies indicated that when Kv3.4 and K44A dynamin 2 were coexpressed without KCNE1, Kv3.4 trafficked efficiently to the cell surface and showed relatively little ER residence (ER-Kv3.4, Pearson's correlation coefficient <0.6; $n = 5$), similar to Kv3.4 colocalization with the ER in the absence of K44A dynamin 2 (Fig. 5, *C* and *E*). When Kv3.4 was coexpressed with both rat KCNE1 and K44A dynamin 2, significant Kv3.4-ER marker colocalization was observed (Pearson's correlation coefficient >0.8; $n = 5$; Fig. 5, *D* and *E*), as seen for Kv3.4 expressed with KCNE1 but without K44A dynamin 2 (Fig. 3, *C* and *D*). However, with K44A dynamin 2 coexpression, some Kv3.4 was also detected at the plasma membrane, not colocalized with KCNE1 (Fig. 5 *D*).

Together, the data suggest that Kv3.4 surface expression is regulated to some extent by DDE, but that this process is not altered by KCNE1 and does not substantially mediate the reduction of Kv3.4 surface expression caused by KCNE1. The relatively minor rescue of Kv3.4 current by K44A dynamin 2, in the presence of KCNE1, is most likely explained by a small fraction of Kv3.4 escaping KCNE1 interaction and thus being available at the surface as homomeric Kv3.4, and susceptible to endocytosis.

DISCUSSION

Fast-inactivating Kv currents are critical determinants of neuronal excitability, modulating action potential repolarization and refractory periods, and interspike intervals by establishing the frequency of spike discharge after depolarization (23,39,40). Here, we demonstrate that KCNE1 and KCNE2 strongly suppress Kv1.4 and Kv3.4 currents (Fig. 1) by sequestering N-type α-subunits intracellularly, early in the secretory pathway (Figs. 2–4). Our findings add to a growing field illustrating the versatility of KCNE subunits in K^+ channel complexes, demonstrating roles outside those first recognized for the founding member, KCNE1, in I_{Ks} complexes with KCNQ1.

Interestingly, although we and others previously found that KCNE1 and KCNE3 seem unable to traffic to the cell surface without heterologous coexpression of an α-subunit partner (22,41), here we found that KCNE2 traffics to the CHO cell surface independently of the coexpressed α-subunit (see Fig. S2 and Fig. S3). This recapitulates the forward trafficking behavior of KCNE2 in HEK293 cells reported by Um and McDonald (36)—who also found that KCNE2 can be exocytosed from the plasma membrane into the extracellular medium. This suggests possible mechanistic differences in the intracellular sequestration of N-type α-subunits by KCNE1 versus KCNE2, because KCNE1 was previously found to travel no farther than the *cis*-Golgi when expressed alone in CHO or COS cells, prompting the suggestion it harbors a Golgi retention, or ER retention/retrieval, motif (22,41).

However, our results suggest that the mechanism for N-type intracellular retention by KCNE1 is not as simple as these α-subunits being unable to chaperone KCNE1 past where it is normally trapped when expressed alone, because KCNE1 is differentially glycosylated depending on Kv3.4 coexpression (Fig. 2 *C*). When alone, KCNE1 is almost exclusively in a high molecular mass form, previously observed for KCNE1 engineered to contain an ER retrieval motif that permits it to reach the Golgi but advance no farther, probably resulting in prolonged exposure to glycosylating enzymes (36,42). In contrast, when coexpressed with Kv3.4, we found KCNE1 is evenly distributed among its non, mono, and biglycosylated forms (Fig. 2 *C*), suggesting it is trafficked somewhat differently when coassembled with Kv3.4—albeit still not traveling farther than the Golgi, aside from a small fraction (~15%; Fig. 5 *B*) that is insufficient to explain this gel migration pattern. We conclude that upon coassembly of KCNE1 or KCNE2 with Kv3.4 or Kv1.4, a retention signal is exposed or formed that is either hidden or absent in homomers of these subunits, or in other complexes they might form (e.g., KCNE3-Kv3.4 or KCNE1-KCNQ1).

Finally, perhaps as an additional control mechanism ensuring efficient prevention of Kv3.4 surface expression, we observe that homomeric Kv3.4 (unlike homomeric KCNQ1 (37)) can be internalized by DDE (Fig. 5, *A*–*C*). The findings are summarized in a model (Fig. 5 *F*). Kv1.4 has also recently been found to undergo clathrin-mediated endocytosis (43). This study further supports the central idea that the versatility of KCNE subunits provides multiple mechanisms for potassium current diversification. In the companion article, a role is demonstrated for N-type suppression by KCNEs in determining the α-subunit composition of surface-expressed channels.

SUPPORTING MATERIAL

Three figures are available at http://www.biophysj.org/biophysj/supplemental/S0006-3495(11)00960-X.

We are grateful to C. Polizoto for critical reading of the article, and thank Drs. G. Kreitzer and R. Levi for thoughtful insights during this project. We thank Dr. Bernardo Rudy for provision of the Kv3.3a clone.

This work was supported by grants HL079275 and HL101190 from the National Institutes of Health/National Heart, Lung, and Blood Institute to G.W.A., who is the recipient of an Irma T. Hirschl Career Scientist Award.

REFERENCES

1. Catterall, W. A. 1984. The molecular basis of neuronal excitability. *Science.* 223:653–661.

2. Yellen, G. 2002. The voltage-gated potassium channels and their relatives. *Nature.* 419:35–42.

3. Coetzee, W. A., Y. Amarillo, …, B. Rudy. 1999. Molecular diversity of K^+ channels. *Ann. N. Y. Acad. Sci.* 868:233–285.
4. Deutsch, C. 2002. Potassium channel ontogeny. *Annu. Rev. Physiol.* 64:19–46.
5. Schwarz, T. L., B. L. Tempel, …, L. Y. Jan. 1988. Multiple potassium-channel components are produced by alternative splicing at the *Shaker* locus in *Drosophila*. *Nature.* 331:137–142.
6. Beck, E. J., R. G. Sorensen, …, M. Covarrubias. 1998. Interactions between multiple phosphorylation sites in the inactivation particle of a K^+ channel. Insights into the molecular mechanism of protein kinase C action. *J. Gen. Physiol.* 112:71–84.
7. Hille, B. 2001. Ion Channels of Excitable Membranes. Sinauer, Sunderland, MA.
8. Mathie, A., J. R. Wooltorton, and C. S. Watkins. 1998. Voltage-activated potassium channels in mammalian neurons and their block by novel pharmacological agents. *Gen. Pharmacol.* 30:13–24.
9. Hoshi, T., W. N. Zagotta, and R. W. Aldrich. 1991. Two types of inactivation in *Shaker* K^+ channels: effects of alterations in the carboxy-terminal region. *Neuron.* 7:547–556.
10. Kurata, H. T., and D. Fedida. 2006. A structural interpretation of voltage-gated potassium channel inactivation. *Prog. Biophys. Mol. Biol.* 92:185–208.
11. Swanson, R., J. Marshall, …, L. K. Kaczmarek. 1990. Cloning and expression of cDNA and genomic clones encoding three delayed rectifier potassium channels in rat brain. *Neuron.* 4:929–939.
12. Sheng, M., M. L. Tsaur, …, L. Y. Jan. 1992. Subcellular segregation of two A-type K^+ channel proteins in rat central neurons. *Neuron.* 9: 271–284.
13. Gan, L., T. M. Perney, and L. K. Kaczmarek. 1996. Cloning and characterization of the promoter for a potassium channel expressed in high frequency firing neurons. *J. Biol. Chem.* 271:5859–5865.
14. Gan, L., and L. K. Kaczmarek. 1998. When, where, and how much? Expression of the Kv3.1 potassium channel in high-frequency firing neurons. *J. Neurobiol.* 37:69–79.
15. Connor, J. A., and C. F. Stevens. 1971. Voltage clamp studies of a transient outward membrane current in gastropod neural somata. *J. Physiol.* 213:21–30.
16. Neher, E. 1971. Two fast transient current components during voltage clamp on snail neurons. *J. Gen. Physiol.* 58:36–53.
17. Hoshi, T., W. N. Zagotta, and R. W. Aldrich. 1990. Biophysical and molecular mechanisms of *Shaker* potassium channel inactivation. *Science.* 250:533–538.
18. Aldrich, R. W., T. Hoshi, and W. N. Zagotta. 1990. Differences in gating among amino-terminal variants of *Shaker* potassium channels. *Cold Spring Harb. Symp. Quant. Biol.* 55:19–27.
19. Tseng-Crank, J., J. A. Yao, …, G. N. Tseng. 1993. Functional role of the NH2-terminal cytoplasmic domain of a mammalian A-type K channel. *J. Gen. Physiol.* 102:1057–1083.
20. Barghaan, J., and R. Bähring. 2009. Dynamic coupling of voltage sensor and gate involved in closed-state inactivation of Kv4.2 channels. *J. Gen. Physiol.* 133:205–224.
21. Lewis, A., Z. A. McCrossan, and G. W. Abbott. 2004. MinK, MiRP1, and MiRP2 diversify Kv3.1 and Kv3.2 potassium channel gating. *J. Biol. Chem.* 279:7884–7892.
22. McCrossan, Z. A., A. Lewis, …, G. W. Abbott. 2003. MinK-related peptide 2 modulates Kv2.1 and Kv3.1 potassium channels in mammalian brain. *J. Neurosci.* 23:8077–8091.
23. Abbott, G. W., M. H. Butler, …, S. A. Goldstein. 2001. MiRP2 forms potassium channels in skeletal muscle with Kv3.4 and is associated with periodic paralysis. *Cell.* 104:217–231.
24. Lee, P. L., J. J. Kohler, and S. R. Pfeffer. 2009. Association of β-1,3-*n*-acetylglucosaminyltransferase 1 and β-1,4-galactosyltransferase 1, *trans*-Golgi enzymes involved in coupled poly-*n*-acetyllactosamine synthesis. *Glycobiology.* 19:655–664.
25. Rajagopalan, L., L. E. Organ-Darling, …, F. A. Pereira. 2010. Glycosylation regulates prestin cellular activity. *J. Assoc. Res. Otolaryngol.* 11:39–51.
26. Di Lorenzo, A., T. D. Manes, …, W. C. Sessa. 2011. Endothelial reticulon-4B (Nogo-B) regulates ICAM-1-mediated leukocyte transmigration and acute inflammation. *Blood.* 117:2284–2295.
27. Saitoh, A., H. W. Shin, …, K. Nakayama. 2009. Three homologous ArfGAPs participate in coat protein I-mediated transport. *J. Biol. Chem.* 284:13948–13957.
28. Bolte, S., and F. P. Cordelières. 2006. A guided tour into subcellular colocalization analysis in light microscopy. *J. Microsc.* 224:213–232.
29. Li, Q., A. Lau, …, E. F. Stanley. 2004. A syntaxin 1, Gα(o), and N-type calcium channel complex at a presynaptic nerve terminal: analysis by quantitative immunocolocalization. *J. Neurosci.* 24:4070–4081.
30. Dunn, K. W., M. M. Kamocka, and J. H. McDonald. 2011. A practical guide to evaluating colocalization in biological microscopy. *Am. J. Physiol. Cell Physiol.* 300:C723–C742.
31. Zagotta, W. N., and R. W. Aldrich. 1990. Voltage-dependent gating of *Shaker* A-type potassium channels in *Drosophila* muscle. *J. Gen. Physiol.* 95:29–60.
32. Fernandez, F. R., E. Morales, …, R. W. Turner. 2003. Inactivation of Kv3.3 potassium channels in heterologous expression systems. *J. Biol. Chem.* 278:40890–40898.
33. Rudy, B., A. Chow, …, E. Vega-Saenz de Miera. 1999. Contributions of Kv3 channels to neuronal excitability. *Ann. N. Y. Acad. Sci.* 868: 304–343.
34. Cartwright, T. A., M. J. Corey, and R. A. Schwalbe. 2007. Complex oligosaccharides are N-linked to Kv3 voltage-gated K^+ channels in rat brain. *Biochim. Biophys. Acta.* 1770:666–671.
35. Iyengar, R., and J. D. Hildebrandt, editors. 2001. G Protein Pathways, Part A: Receptors, Volume 343 (Methods in Enzymology). Academic Press, San Diego, CA.
36. Um, S. Y., and T. V. McDonald. 2007. Differential association between HERG and KCNE1 or KCNE2. *PLoS ONE.* 2:e933.
37. Xu, X., V. A. Kanda, …, G. W. Abbott. 2009. MinK-dependent internalization of the I_{Ks} potassium channel. *Cardiovasc. Res.* 82:430–438.
38. Zhang, J., L. S. Barak, …, S. S. Ferguson. 1997. A central role for β-arrestins and clathrin-coated vesicle-mediated endocytosis in β2-adrenergic receptor resensitization. Differential regulation of receptor resensitization in two distinct cell types. *J. Biol. Chem.* 272:27005–27014.
39. Riazanski, V., A. Becker, …, H. Beck. 2001. Functional and molecular analysis of transient voltage-dependent K^+ currents in rat hippocampal granule cells. *J. Physiol.* 537:391–406.
40. Pannaccione, A., F. Boscia, …, L. Annunziato. 2007. Up-regulation and increased activity of Kv3.4 channels and their accessory subunit MinK-related peptide 2 induced by amyloid peptide are involved in apoptotic neuronal death. *Mol. Pharmacol.* 72:665–673.
41. Chandrasekhar, K. D., T. Bas, and W. R. Kobertz. 2006. KCNE1 subunits require co-assembly with K^+ channels for efficient trafficking and cell surface expression. *J. Biol. Chem.* 281:40015–40023.
42. Krumerman, A., X. Gao, …, T. V. McDonald. 2004. An LQT mutant MinK alters KvLQT1 trafficking. *Am. J. Physiol. Cell Physiol.* 286:C1453–C1463.
43. McKeown, L., V. C. Jones, and O. T. Jones. 2009. PIN-G reporter for imaging and defining trafficking signals in membrane proteins. *Methods Mol. Biol.* 574:235–248.